Proceedings of Global Power and Propulsion Society
ISSN-Nr: 2504-4400
GPPS Xi'an21
18th–20th October, 2021

www.gpps.global

GPPS-TC-2021-0075

EFFECTS OF SURFACE ROUGHNESS ON FLOW LOSSES OF A HIGH-LOADING LOW-PRESSURE TURBINE CASCADE

Xian Zeng
Zhejiang University
zzz3331010@zju.edu.cn
Hangzhou, Zhejiang, China

Jiaqi Luo
Zhejiang University
jiaqil@zju.edu.cn
Hangzhou, Zhejiang, China

ABSTRACT

Laminar separation induced flow transition has been regarded as one common but complex flow in low pressure turbine (LPT), which is one main source of flow losses of LPT. Lots of studies have demonstrated that the realistic rough blade of LPT favors the reduction of flow losses as the laminar separation can be delayed by increasing the roughness. Subsequently, the flow separation bubble on the suction side can be reduced, and even disappears. The present paper investigates the effects of surface roughness on flow separation of an LPT cascade, T106C. Firstly, a detailed grid-independent study assisted by Richardson extrapolation is presented to illustrate the reliability of the numerical solutions obtained by solving RANS and SST γ-$R\tilde{e}_\theta$ transition model equations. Then a series of roughness with different geometric roughness height (Ra) are imposed on the whole suction side. The effects of roughness on the reduction of separation bubble are illustrated and compared. The results demonstrate that there is one critical Ra, below which the flow losses decrease, while above which the flow losses increase as Ra increases. Finally, different roughness allocations with sand grains imposed on different blade portions of the suction side are studied. Through comparisons, the sensitivities of flow loss reduction to the roughness on different blade portions are evaluated and illustrated. The study paves the way for finding an optimal roughness allocation on the suction side to minimize the flow losses.

Keywords: Low pressure turbine; Roughness; Flow loss; Flow separation; Transition

INTRODUCTION

The low pressure turbine (LPT), as the heaviest component in aero engines, takes up to one third of the total weight of the core engine. High-loading blade design is one well-recognized method to reduce the weight and fuel consumption of the engine. At the same time, this design increases the aerodynamic load of each blade, leading to stronger adverse pressure gradients in the expansion section of LPT. Under the condition of low Reynolds number (Re), stronger adverse pressure gradient will increase the possibility of flow separation and transition in boundary layer, resulting in higher profile loss. Therefore, separation and transition control are significant for LPT. Since Stieger (Stieger, 2002), Zhang (Zhang, 2006) had studied flow control on LPT blades in unsteady flow, research on the influence of vortex generator jets (Sondergaard et al., 2002), unsteady wakes (Ciorciari et al., 2014)(Sinkwitz et al., 2019), and contoured endwall (Qu et al., 2019) on separation transition and secondary flow has been rapidly carried out.

Compared to other flow control methods, surface roughness, a universal factor in engineering, can affect flow separation and transition without increasing the structural complexity. Besides, during the service period of LPT, corrosion and deposition can significantly increase the surface roughness (Kellersmann et al., 2018). Consequently, analysis and evaluation of performance impact on the flow separation and transition due to surface roughness is of utmost importance to the design of LPT blade.

Nikuradse and Schlichting (Nikuradse, 1933)(Schlichting, 1979) pioneered investigating the impact of surface roughness initially. Nikuradse conducted the classic sandgrain-roughened pipe flow experiment, Schlichting reported the analyses and proposed the concept of 'equivalent sand roughness', k_s, which correlates the skin friction of any roughness to a sand grain roughness with the same skin friction. The concept has been widely used in both scientific and industrial communities. And various approaches based on experiment data have been given to convert roughness parameters to equivalent sand roughness.

Over the years, many scientific researches have studied the effects of surface roughness on the aerodynamic performance of turbomachinery by both experiments and numerical simulations. Bammert and Sandstede (Bammert and Sandstede, 1980) focused on boundary layer development on a rough turbine blade and found the momentum thickness of roughness surface is about three times as that of the smooth surface. Kind et al. (Kind et al., 1998) studied the effects of roughness on static pressure distribution for a planar turbine cascade in incompressible flow. Hummel et al. (Hummel et al., 2005) found that the profile loss caused by surface roughness increases as (Re) increases. Roberts and Yaras (Roberts and Yaras, 2005)(Roberts and Yaras, 2006) illustrated that surface roughness and free-stream turbulence have comparable effects on the location of transition inception in separation bubbles. Besides, they measured separation-bubble transition over a range of surface with randomly distributed roughness elements, which approximately represents the realistic conditions of turbine blades in service. As a result, the effects of roughness spacing and skewness are found to be small by comparing whit those of roughness height. Joo et al. (Joo et al., 2016) modelled surface roughness by regularly placing roughness elements on the suction side of LPT. Kellersmann et al. (Kellersmann et al., 2018) emphasized the importance of roughness-induced loss in LPT and illustrated that the influence of surface roughness on the turbine efficiency is significant at take-off but negligible at cruise.

The impact mechanisms of surface roughness of LPTs under low Re have not been reported yet. Furthermore, whether it is possible to effectively control the separation and transition under low Re by allocating roughness on the suction side of LPT blade requires to be further studied. In this paper, the effects of surface roughness on flow losses of a typical LPT cascade, T106C are studied by solving RANS and SST γ-$R\tilde{e}_\theta$ transition model equations. The reliability of numerical simulations is verified and validated by a detailed grid-independent study assisted by Richardson extrapolation. With different roughness imposed on the suction side, a detailed numerical analysis of T106C is performed. Besides, different roughness allocations are imposed on the suction side to illustrate the sensitivities of flow loss reduction to the roughness change.

NUMERICAL SIMULATION

The specifications of T106C are listed in Table 1. The profile is presented in Fig 1.

Table 1 Specifications of T106C cascade

Parameters	Unit	Value
Pitch	[mm]	189.6
Span	[mm]	375.0
Design Inlet Flow Angle	[°]	32.7
Design Exit Flow Angle	[°]	-63.2
Exit Isentropic Mach Number		0.65

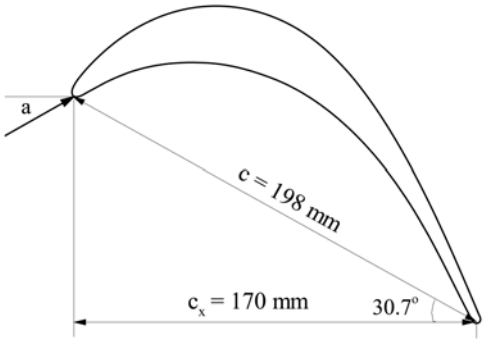

Figure 1 Profile of T106C cascade

According to Mich*á*lke et al.'s experiments (Michálek et al., 2012), Re can be matched by adjusting the inlet total pressure and the outlet static pressure, while the isentropic Mach number at the outlet remains constant. In this paper, two Re conditions with different-length separation bubbles are selected from experiment data. Under the condition of $Re = 2.5 \times 10^5$, the separation bubble is stable and shortest among those in experiment study. Under the condition of $Re = 1.4 \times 10^5$, the separation bubble is longer and in a critical state. Because as Re decreases to be lower, the separation bubble cannot be closed on the suction side and the so-called "open bubble" appears. Besides, the experimental results are sufficient at these two Reynolds number. The boundary conditions of two Re are provided in Table 2. In addition, in order to maintain the same free-stream turbulence intensity as the experiment, the inlet turbulence intensity is 0.96% in this study.

Table 2 Boundary conditions

$Re_{is,out}/10^3$	Pt_{in}/Pa	Tt_{in}/K	Ps_{out}/Pa
250	14298.5	293	10764.5
140	8007.3	293	6028.1

Two-dimensional steady Reynolds-averaged Navier-Stokes (N-S) equations are solved to simulate the flow on a multi-block grid. The computational fluid dynamics (CFD) software ANSYS-Fluent is used. The Shear stress transport (SST) turbulence model and γ-$\tilde{Re}_\theta$ transition model with roughness correlation are used throughout the work. The flow at the inlet is subsonic. The flow angle and total temperature at the inlet are all given as 32.7° and 288.15K, respectively. The static pressure at the outlet is given according to the maintained isentropic Mach number, 0.65. The maximum non-dimensional wall distance of the first cell to the blade surface y^+ is below 1. And the computational domain and grid is showed in Fig 2.

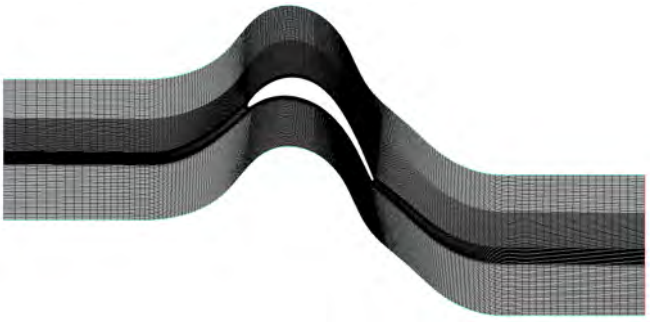

Figure 2 Computational domain and grid

Before investigating the effect of surface roughness on flow losses of T106C, the numerical simulation method is verified and validated by a generalized Richardson extrapolation (GRE) method, which is an error estimator based on the mixed-order analysis (Roy, 2003). This error estimator can provide good estimates of the actual error. For every three grids, the approximate exact solutions can be calculated by GRE. In the study, the total pressure at the outlet is calculated on five grids, as shown in Fig 3. The calculated results are compared with the one obtained from GRE. It is clear that the calculated results of the third grid is already very close to the GRE one.

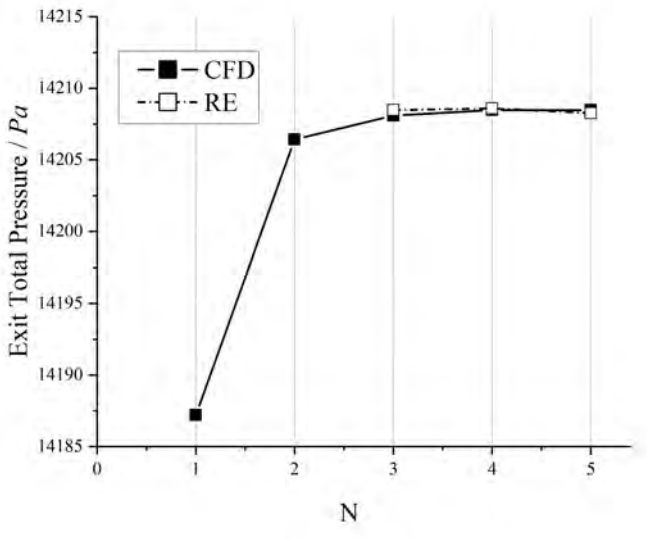

Figure 3 Grid-independent solutions of outlet total pressure

Validation is also necessary to confirm the reliability of numerical results. The isentropic Mach number on the blade is shown and compared with the experiments (Michálek et al., 2012) in Fig 4. Generally, the numerical solutions of grid 3 and grid 4 are almost duplicates of each other, and are both close to the experiment ones. In the following study, the third grid with a resolution, 8×10^4 will be used. Besides, at low Re as shown in Fig 4a), the predicted separation bubble is

smaller than the one of experiment. At the relative high Re, as shown in Fig 4b), the predicted separation bubble matches the experiment one better.

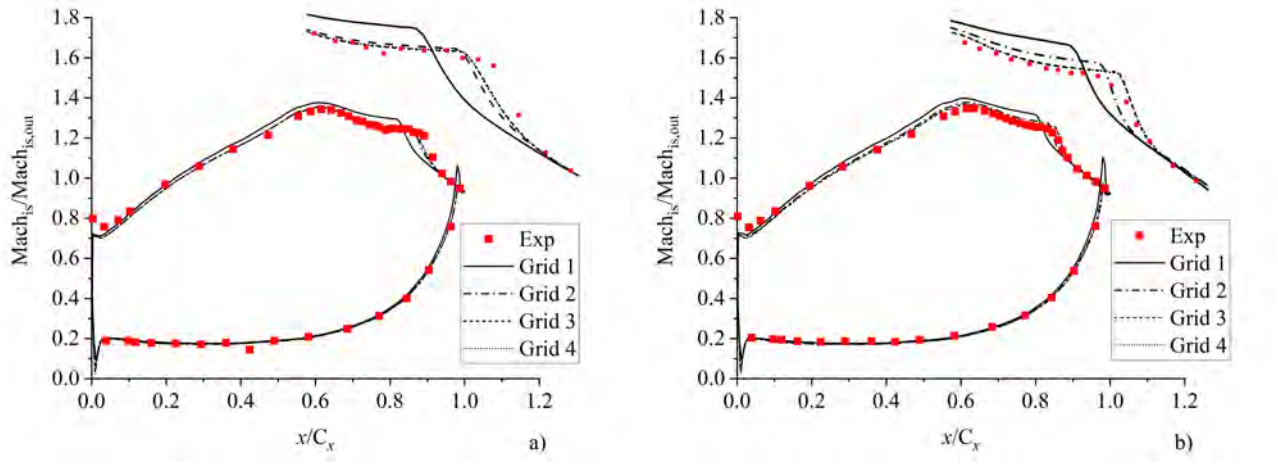

Figure 4 Isentropic Mach number distributions on the blade: a) $Re = 1.4 \times 10^5$**; b)** $Re = 2.5 \times 10^5$

The mass-averaged kinetic energy loss coefficient (KELC) is calculated at the outlet of the cascade. The definition of KELC is:

$$\zeta = 1 - \frac{1 - \left(\frac{p_2}{p_{02}}\right)^{\frac{\kappa-1}{\kappa}}}{1 - \left(\frac{p_2}{p_{01}}\right)^{\frac{\kappa-1}{\kappa}}} \tag{1}$$

where the p and p_0 are static pressure and total pressure, respectively, the subscripts 1, 2 indicate the inlet and outlet boundaries, respectively, κ is the ratio of specific heat. The KELC at $Re = 1.4 \times 10^5$ and $Re = 2.5 \times 10^5$ are given in Table 3.

Table 3 Comparisons of KELC

Re	$\zeta - EXP/\%$	$\zeta - CFD/\%$	$Error/\%$
250000	2.22	2.15	-3.15
140000	3.43	3.07	-10.50

At high Re, the numerical KELC is more consistent with the experiment. Besides, KELC increases as Reynold number decreases. In fact, the experiments (Michálek et al., 2012) illustrated that as Reynolds number decreases, the size of separation bubble increases. At ultra-low Re, the open separation bubble appears on the suction side, making the prediction of flow separation and transition more challenging by numerical simulation. Mentioned that although the relative deviation exceeds 10% at $Re = 1.4 \times 10^5$, it is still below the measurement uncertainty. In Michálke's experiment study, the uncertainty of KELC is 20%. In the study, the effects of surface roughness will be studied at $Re = 2.5 \times 10^5$. Mentioned that in the numerical simulation, the roughness of the blade used in the experimental study cannot be determined and thus it is not taken into account. In fact, if the roughness of the blade is dominated by manufacturing, the roughness is quite possibly within the hydrodynamic smooth regime, the effects of which are negligible.

ROUGHNESS DESCRIPTIONS

In order to effectively illustrates the impact of roughness on flow separation and transition, eleven different sizes of roughness covering almost the whole variation range of realistic roughness of LPT are studied. The roughness is usually virtually measured by a non-dimensional parameter, k^+ (Schlichting, 1979), the definition of which is:

$$k^+ = \mathrm{Re}\frac{k_S}{C}\sqrt{\frac{C_f}{2}} \tag{2}$$

$$C_f = \left(2.87 + 1.58 \lg \frac{C}{k_s}\right)^{-2.5} \tag{3}$$

where k_s is the equivalent sand roughness, which can be approximately calculated by $k_s = 6.2Ra$, as suggested by Koch et al. (Koch and Smith, 1976); Re is the Reynolds number based on the inlet flow velocity and blade chord; C_f is the skin friction coefficient and C is the chord. The elven roughness sizes are listed in Table 4.

Table 4 Roughness sizes

k^+	3	8	15	30	45	60	75	90	105	120	150
$Ra/\mu m$	8	19	34	63	91	117	143	168	192	216	263

The influence of roughness on the pressure side flow is neglectable for the overall performance of LPT (Kellersmann et al., 2018). In this paper, roughness with different geometric roughness height (Ra) is allocated on the suction side of the smooth blade. The position of separation onset, transition onset and transition end are significant to the laminar separation transition process. Besides, Zhang's study of surface trips on LPT(Zhang, 2006) demonstrated that the surface trip located on the portions from velocity peak to separation onset can further reduce the profile losses, implying that the position of velocity peak is one additional critical position. In order to evaluate the sensitivities of flow loss reduction to the roughness for different blade portions, four roughness allocations (Type A, B, C and D) are given. Under the same Re, the positions of suction velocity peak (P), laminar separation (S), transition onset (T'), transition end (T), and reattachment (R) are evaluated on the smooth surface. Roughness allocations are given in Fig 5.The roughness elements are imposed on the blade portions from leading edge (LE) to the trailing edge (TE), transition onset, laminar separation and suction velocity peak for Type A, Type B, Type C and Type D, respectively.

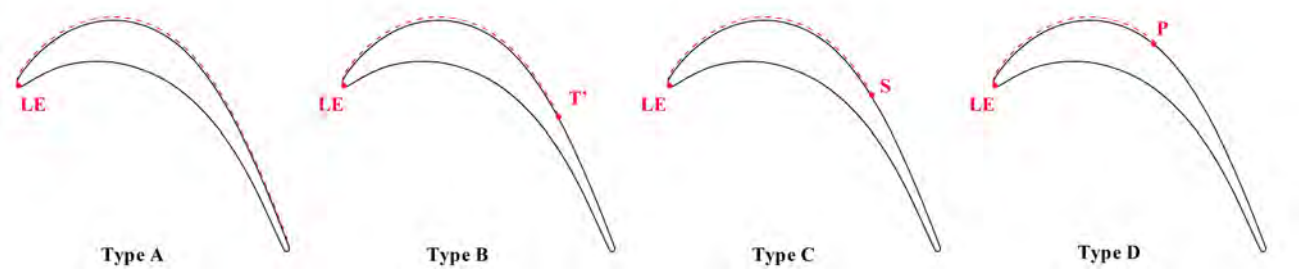

Figure 5 Roughness allocations on the suction side

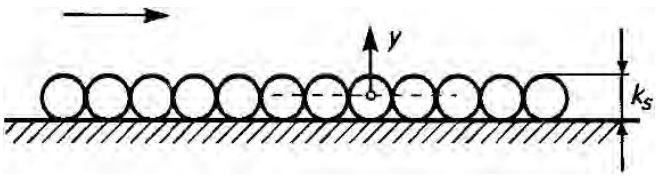

Figure 6 Illustration of equivalent sand-grain roughness

Taking into account the effects of surface roughness in numerical simulation by CFD, the equivalent sand-grain roughness has been applied(Schlichting, 1979). Fig. 6 illustrates the schema of equivalent sand-grains imposing on the smooth wall, where the wall is uniformly covered by a layer of spheres to approximately represent the actual roughness with different shapes and sizes. Moreover, it is assumed that the roughness induces flow blockage as the flow passage decreases by 50% of the height of roughness elements. In such cases, the displacement caused by the surface roughness results in a corrected non-dimensional distance y_c^+ for the first grid away from the wall

$$y_c^+ = y^+ + k_s^+/2 \tag{4}$$

where k_s^+ is the non-dimensional equivalent sand roughness. Therefore, the law-of-the-wall for mean velocity modified for roughness wall can be applied correctly. By this corrected law-of-the-wall, flow computations as introduced in the Section "Numerical Simulation" can be accomplished more efficient and easier because it is not necessary to describe the actual roughness elements by grids.

RESULTS AND DISCUSSION

KELC with respect to the eleven different roughness sizes as shown in Table 4 are obtained and presented in Fig 7 for all the four roughness allocations. The results demonstrate that as k^+ increases, the flow losses firstly decrease and then increase abruptly and significantly. It is clear that a critical k^+ exists and it is about 75 in the present study. The

variations of KELC versus k^+ are consistent with the current roughness impact theory (Schlichting, 1979), which says that the performance impact of roughness is not a single function of k^+ but depends on the value of k^+. Based on the theory, the roughness can be categorized by three distinct types: hydrodynamically smooth, transitional and fully rough. To better illustrates the variations of KELC, the results are locally enlarged and given in Fig 7b). When k^+ is lower than 5, the roughness is within the hydrodynamically smooth regime and the impact on KELC are almost the same for the four roughness allocations. As k^+ increases in the transitional regime, Type B is the most efficient to reduce KELC. When k^+ is in the full rough regime, KELC increases as k^+ increases. Moreover, since the roughness is imposed on the whole suction side, KELC of Type A is the highest. For Type D with the roughness are imposed on the blade portions from LE to the suction velocity peak, KELC is the lowest.

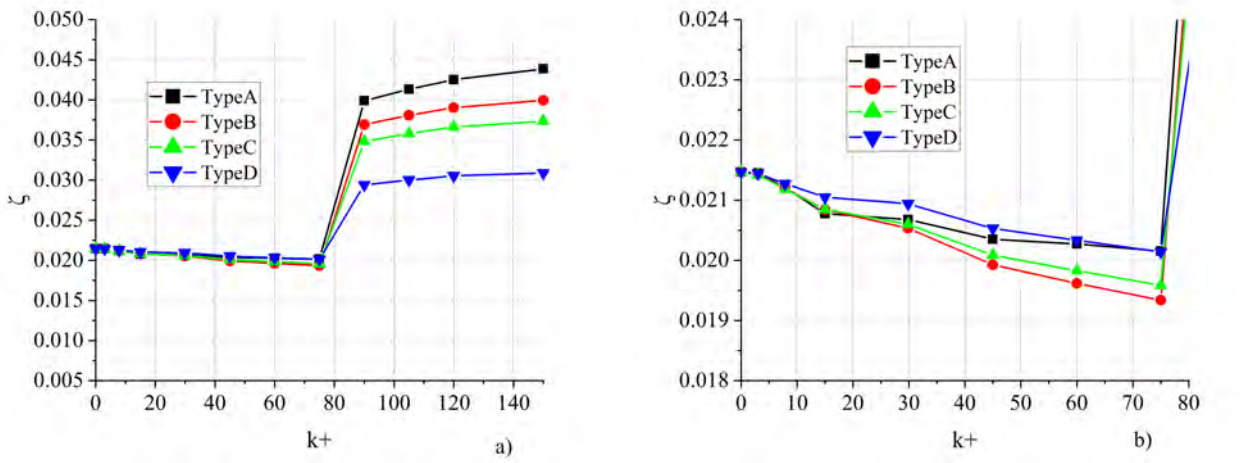

Figure 7 Variations of KELC versus k^+: a) global; b) locally enlarged

In order to illustrate the development of boundary layer and the effects of k^+ on the variations of KELC, isentropic Mach number distributions on the suction side for four different roughness sizes of Type A are given in Fig 8. From Fig 8a) it can be found that as k^+ increases, the separation bubble on the suction side moves downstream. For $k^+ = 120$, the separation bubble disappears and the flow is turbulent, which can be further verified by Fig 8b) and Fig 8c). In Fig 8b), the skin friction coefficient, C_f of $k^+ = 120$ is far higher than others, where C_f is defined as the ratio of local wall shear stress to dynamic head. In Fig 8c), the abrupt increase of intermittency indicates flow transition. It is clear that as k^+ increases, the position of transition onset moves downstream and the maximum intermittency increases. When $k^+ = 120$, the intermittency is unit on the suction side, indicating that the turbulent flow is already fully developed. It is well known that the skin friction is zero at the positions of flow separation and reattachment. In Fig 8b), the separation point and reattachment point move downstream, compared with the smooth surface. The distance between the two points decreases as k^+ increases, demonstrating that the separation bubble is shortened, which favors the decrease of flow loss. As the separation bubble moves downstream as shown in Fig 8a), the position of transition onset also moves downstream as k^+ increases. Furthermore, the maximum intermittency increases as k^+ increases, implying that flow transition intensifies. The approximate positions of the critical points including flow separation, transition onset, transition end and reattachment are given in Table 5, from which the length of separation bubble is estimated.

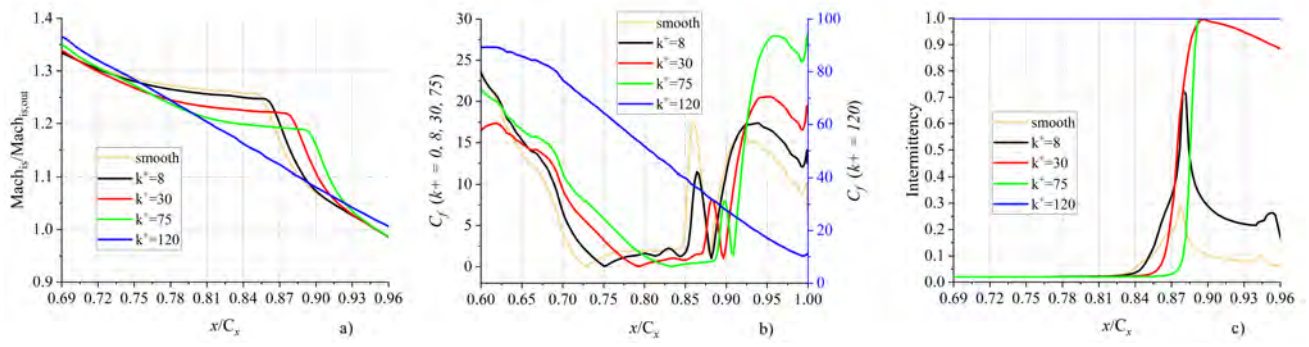

Figure 8 Distribution of flow variables on the blade: a) isentropic Mach number: b) skin friction coefficient; c) intermittency

Table 5 Positions of the critical points on the suction side for Type A

k^+	$S(x/C_f)$	$T'(x/C_f)$	$T(x/C_f)$	$R(x/C_f)$	$Length(x/C_f)$
smooth	0.73	0.83	0.85	0.88	0.15
8	0.75	0.84	0.86	0.88	0.13
30	0.79	0.85	0.87	0.90	0.11
75	0.82	0.87	0.89	0.91	0.09
120	/	/	/	/	/

From Fig 8 it is known that as k^+ increases, the positions of flow separation and transition onset move downstream. It can be easily understood that for the laminar separation and transition boundary flow, the increased roughness strengthens the turbulence intensity and the laminar separation can be effectively suppressed and delayed. Besides, attributed to the strengthened turbulence intensity, the transition of laminar flow is more easily achieved. As showed in Table 5, although the position of transition onset moves downstream along with the separation bubble, the distance between separation point (S) and transition onset (T') decreases as k^+ increases. The results further confirm that the increased roughness favors flow transition in the laminar separation and transition boundary layer flow of LPT.

Besides the roughness size, the roughness allocation also has significant influence on flow losses by affecting flow separation and transition in the boundary layer. Under the condition that $Re = 2.5 \times 10^5$, the effects of the aforementioned four roughness allocations on the development of boundary layer and thus KELC are carefully presented and compared.

Fig 9 and Fig 10 present the distributions on the suction side of isentropic Mach number and skin friction coefficient at $k^+ = 8$ and $k^+ = 30$, respectively. It is clear that when k^+ is low, the distributions of Type A, Type B and Type C are almost duplicates, while the distributions of Type D are quite different. Generally, the positions of the critical points of Type D in Fig 9 and Fig 10 are both close to those points on the smooth surface listed in Table 5. Compared with the smooth surface, the separation bubbles of Type A, Type B and Type C moves downstream obviously, but the separation bubble of Type D locates upstream of the former three. In such cases, the contributions of Type D to KELC reduction should be the most ordinary, which can be in fact confirmed by Fig 7.

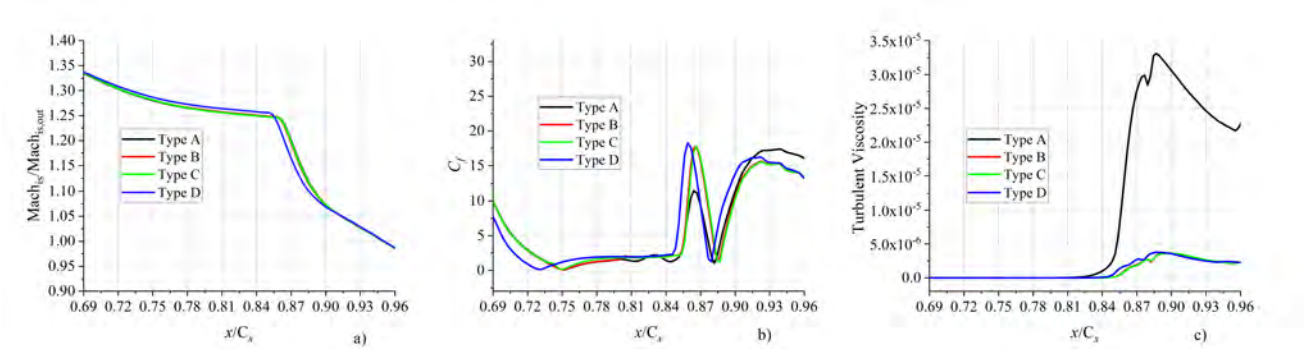

Figure 9 Distributions of flow variables on the blade for $k^+ = 8$: a) isentropic Mach number: b) skin friction coefficient; c) turbulent viscosity.

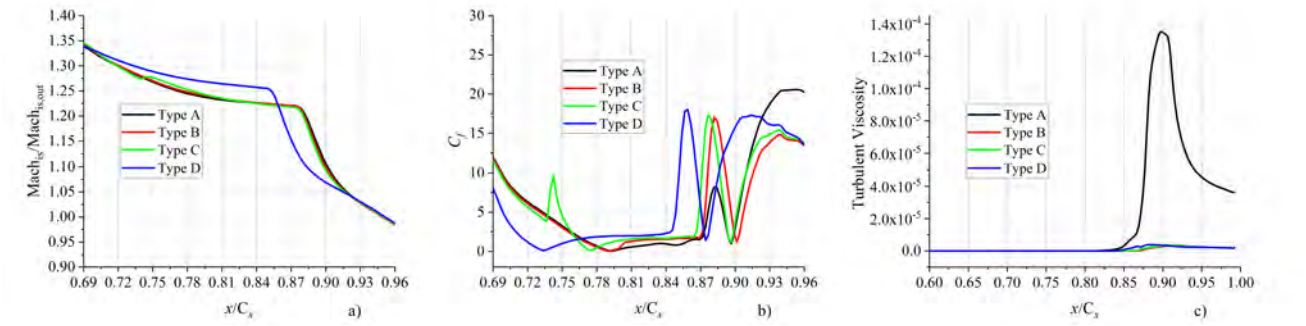

Figure 10 Distributions of flow variables on the blade for $k^+ = 30$: a) isentropic Mach number: b) skin friction coefficient; c) turbulent viscosity.

In addition, at $k^+ = 8$, the positions of separation point and reattachment for Type A, Type B and Type C are quite

close, resulting in almost the same reductions of KELC as shown in Fig 7. At $k^+ = 30$, the separation points of Type A and Type B locate downstream of that of Type C, while the reattachment point of Type B is slightly downstream of those of Type A and Type C. In such cases, the separation bubble of Type A is shortest and the one of Type B is shorten than Type C. Subsequently, KELC of Type B is lower than that of Type C. Mentioned that the roughness is imposed on the whole suction side for Type A. The increased roughness on the blade portions within fully developed turbulent flow inevitably increases the flow loss. In both Fig 9c) and Fig 10c), the turbulent viscosity on the rear portions of suction side for Type A is highest among the four.

As k^+ increases, the differences between different types of roughness allocations are clearer. For $k^+ = 75$ as shown in Fig 11, the separation bubble of Type D is still upstream of those of other types. The separation bubbles of Type A and Type B are close to each other and are downstream of that of Type C. From Fig 11b) it can be further confirmed that the separation bubble of Type B is shortest, implying that KELC of Type B is the lowest, as shown in Fig 7. Similar to Fig 10, due to the increased roughness on the rear portions of the suction side, the turbulent flow downstream the reattachment point is intensified, resulting in increased KELC for Type A. From Fig 11c) it can be found that the turbulent viscosity for Type A is highest on the rear portions of the suction side.

From the results shown by Fig 10 and Fig 11, it can be found that when k^+ is within the transitional regime, the roughness allocation Type B is the most effective to reduce the flow losses. However, the roughness allocation Type D has the fewest contributions to the reductions of flow losses. In such situations, the blade portions from suction velocity peak to transition onset with roughness imposed on contribute the most reductions to flow losses.

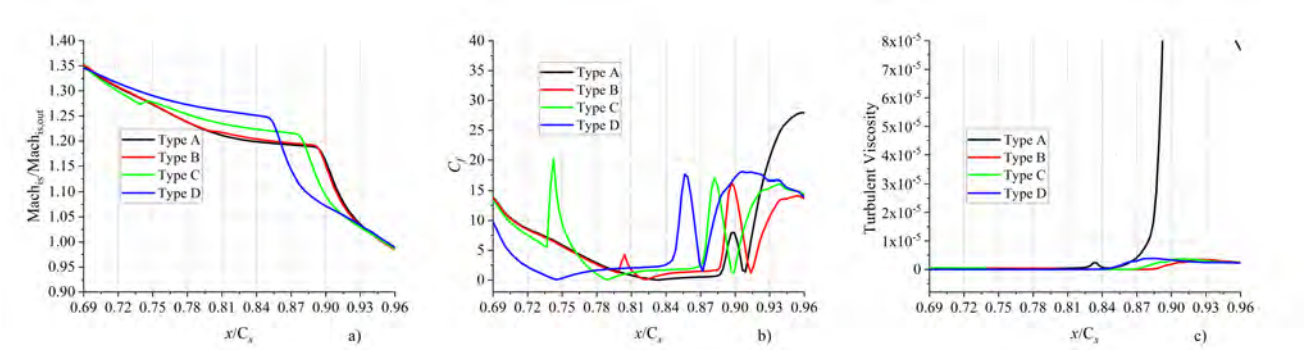

Figure 11 Distributions of flow variables on the blade for $k^+ = 75$: a) isentropic Mach number; b) skin friction coefficient; c) turbulent viscosity.

When $k^+ = 120$, the separation bubble on the suction side already disappears for all the four roughness allocations. The flow on the rear portions of the suction side is turbulent. The distributions of isentropic Mach number of the four types are close, as shown by Fig 12a). In such situations, KELC only depends on the roughness allocation, i.e., the blade portions with roughness imposed on. As introduced in the section of roughness descriptions, the roughness is imposed on the portions from LE to the critical points of TE, transition onset, separation and suction velocity peak for Type A, Type B, Type C and Type D, respectively. From Fig 12b) and Fig 12c) it can be found that both the skin friction coefficient and turbulent viscosity abruptly and significantly decrease at the critical points for Type B, Type C and Type D. The results demonstrate once more that the increased roughness intensifies the turbulent flow when k^+ is within the full turbulent regime.

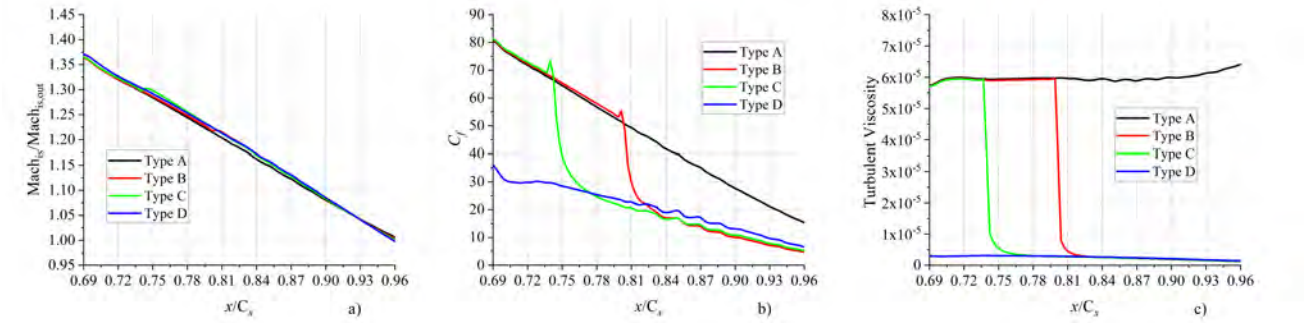

Figure 12 Distributions of flow variables on the blade for $k^+ = 120$: a) isentropic Mach number; b) skin friction coefficient; c) turbulent viscosity.

CONCLUSION

The results are presented and compared in detail. The effects of roughness size, roughness allocation on the reduction of flow losses are illustrated.

(1) There is a critical k^+, below which the separation bubble shortens and the flow losses decrease as k^+ increases, while above which the separation bubble disappears and the flow losses increase as k^+ increases. That's because the flow is already turbulent when k^+ is within the full turbulent regime. The increased k^+ intensifies the turbulence.

(2) Considering the impact of different roughness allocations, the critical points of transition onset, reattachment move downstream and the length of separation bubble varies when k^+ is within the transitional regime. Roughness allocation from LE to suction velocity peak has the fewest contributions to the reductions of flow losses, while the roughness allocation from LE to transition onset has the most contributions. Due to the increased turbulent flow loss on the rear portions of the suction side, roughness allocation on the whole suction side has fewer contributions to the reductions of flow losses. The laminar separation and transition flow loss of T106C is the most sensitive to the roughness variations on the blade portions from suction velocity peak to transition onset.

ACKNOWLEDGMENTS

The authors like to thank The National Natural Science Foundation of China (Grant nos. 51676003, 51976183) and National Science and Technology Major Project of China (Grant no. J2019-II-0012-0032) for support the research.

References

Bammert, K. and Sandstede, H. (1980), 'Measurements of the boundary layer development along a turbine blade with rough surfaces', *Journal of Engineering for Gas Turbines and Power* **102**(4), 978–983.

Ciorciari, R., Kirik, I. and Niehuis, R. (2014), 'Effects of Unsteady Wakes on the Secondary Flows in the Linear T106 Turbine Cascade', *Journal of Turbomachinery* **136**(9). 091010.

Hummel, F., Lötzerich, M., Cardamone, P. and Fottner, L. (2005), 'Surface roughness effects on turbine blade aerodynamics', *Journal of Turbomachinery* **127**(3), 453–461.

Joo, J., Medic, G. and Sharma, O. (2016), Large-Eddy Simulation Investigation of Impact of Roughness on Flow in a Low-Pressure Turbine, Vol. Volume 2C: Turbomachinery of *Turbo Expo: Power for Land, Sea, and Air*. V02CT39A053.

Kellersmann, A., Weiler, S., Bode, C., Friedrichs, J., Städing, J. and Ramm, G. (2018), 'Surface Roughness Impact on Low-Pressure Turbine Performance Due to Operational Deterioration', *Journal of Engineering for Gas Turbines and Power* **140**(6). 062601.

Kind, R. J., Serjak, P. J. and Abbott, M. W. P. (1998), 'Measurements and prediction of the effects of surface roughness on profile losses and deviation in a turbine cascade', *Journal of Turbomachinery* **120**(1), 20–27.

Koch, C. C. and Smith, L. H. (1976), 'Loss sources and magnitudes in axial-flow compressors', *Journal of Engineering for Gas Turbines and Power* **98**(3), 411–424.

Michálek, J., Monaldi, M. and Arts, T. (2012), 'Aerodynamic Performance of a Very High Lift Low Pressure Turbine Airfoil (T106C) at Low Reynolds and High Mach Number With Effect of Free Stream Turbulence Intensity', *Journal of Turbomachinery* **134**(6). 061009.

Nikuradse, J. (1933), 'Laws of flow in rough pipes', *VDI-Forschungsheft* **361**(Series B), VOL. 4. (English translation NACA-TM-1292, 1950).

Qu, X., Zhang, Y., Lu, X., Lei, Z. and Zhu, J. (2019), 'Effect of periodic wakes and a contoured endwall on secondary flow in a high-lift low-pressure turbine cascade at low reynolds numbers', *Computers & Fluids* **190**, 1–14.

Roberts, S. K. and Yaras, M. I. (2005), 'Boundary-layer transition affected by surface roughness and free-stream turbulence', *Journal of Fluids Engineering* **127**(3), 449–457.

Roberts, S. K. and Yaras, M. I. (2006), 'Effects of surface-roughness geometry on separation-bubble transition', *Journal of Turbomachinery* **128**(2), 349–356.

Roy, C. J. (2003), 'Grid convergence error analysis for mixed-order numerical schemes', *AIAA Journal* **41**(4), 595–604.

Schlichting, H. (1979), *Boundary-layer theory*, 7th edn, McGraw-Hill, New York.

Sinkwitz, M., Winhart, B., Engelmann, D., di Mare, F. and Mailach, R. (2019), 'Experimental and Numerical Investigation of Secondary Flow Structures in an Annular Low Pressure Turbine Cascade Under Periodic Wake Impact—Part 1: Experimental Results', *Journal of Turbomachinery* **141**(2). 021008.

Sondergaard, R., Rivir, R. B. and Bons, J. P. (2002), 'Control of low-pressure turbine separation using vortex-generator jets', *Journal of Propulsion and Power* **18**(4), 889–895.

Stieger, R. D. (2002), The effect of wakes on separating boundary layers in low pressure turbines, PhD thesis, University of Cambridge.

Zhang, X. F. (2006), Separation and transition control on ultra-high-lift low pressure turbine blades in unsteady flow, PhD thesis, University of Cambridge.